3 Orbit Measurement and Correction

In practice, there are many uncertainties whose presence must be appreciated when correcting the beam orbit in both linear and circular accelerators. Such uncertainties include the variations in the electronic and/or mechanical centers of the beam position monitors (BPMs), in the magnetic center of the quadrupoles (inside which the position monitors are often mounted), or in the electromagnetic center of accelerating structures. Consider the case illustrated in Fig. 3.1. In this case, the absolute beam position, with respect to a reference axis, is given by

$$x = x_d + x_b + x_m \,, \tag{3.1}$$

where x_d represents the quadrupole offset from the reference axis, x_b gives the offset of the electronic center of the BPM relative to the quadrupoles, and x_m denotes the measurement from the BPM. The reference axis may be chosen to minimize emittance dilutions in a global sense. In the ideal case for which the reference axis is straight and in the center of all quadrupoles, a typical most simple steering algorithm aimed towards zeroing the BPM readings would

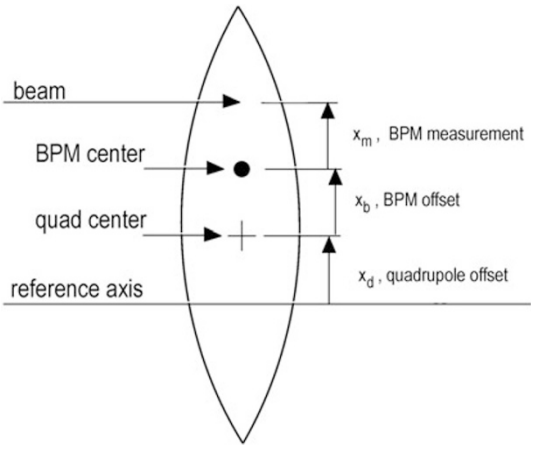

Fig. 3.1. Sketch showing relative positions of the BPM, the quadrupole, and the beam position measurement from an ideal reference axis (Courtesy C. Adolphsen, 1999)

M. G. Minty et al., *Measurement and Control of Charged Particle Beams,*
https://doi.org/10.1007/978-3-662-08581-3_3

still place the beam off-axis in the quadrupole if $x_b \neq 0$. For accelerators with tight emittance budgets and correspondingly tight alignment tolerances, clearly more sophisticated steering algorithms are needed.

If the orbit is off-center in a quadrupole magnet, dispersion is generated, and, in a ring, also the beam energy may be changed or the polarization may decrease. An orbit that is off-center in a sextupole induces skew coupling and/or beta beating. Thus it is very important to center the orbit in these magnets. The standard tools for correcting the orbit are corrector dipoles. Of course, such an orbit correction will never be perfect. Figure 3.2 shows a typical absolute orbit reading from the PEP-II HER, after moderate orbit correction during commissioning.

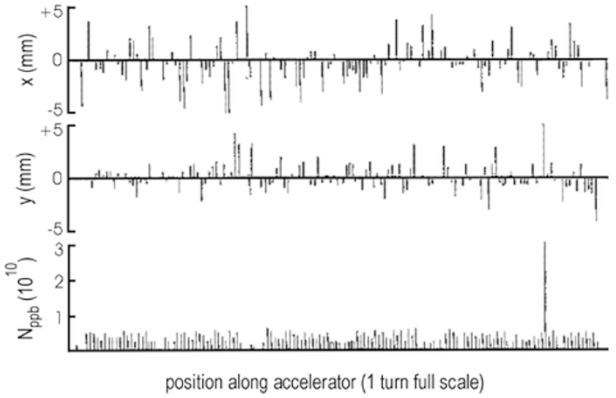

Fig. 3.2. Typical commissioning orbit in the PEP-II HER: (*top*) horizontal orbit in mm; (*center*) vertical orbit in mm; (*bottom*) intensity in 10^{10} (Courtesy U. Wienands, J. Seeman *et al*, 1998)

We will see that if the BPM offsets are not known, and possibly larger than the alignment errors, a better strategy for optimal emittance preservation is to reduce the rms strength of the steering correctors, and to pay less attention to the absolute orbit reading. In several cases, at the SLC and at the ATF, this second approach significantly reduced the magnitude of the residual vertical dispersion [1]. Sometimes other constraints are imposed on the orbit. For example, a certain orbit amplitude or a certain angle may be desired near the injection or extraction points, or near a synchrotron light beamline. In such cases, a constant orbit must be maintained at the adjacent BPMs.

Increased beam emittances may arise from beam-to-magnet or beam-to-structure position deviations as shown conceptually in Fig. 3.3. The beam passing through a single misplaced quadrupole experiences the next lower-order field namely a dipole field. The misalignment therefore generates a betatron oscillation *and* dispersion as higher energy particles are less deflected by the dipole field. Also in the case of a displaced structure a betatron os-

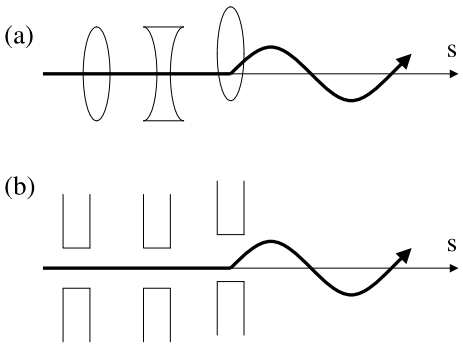

Fig. 3.3. Conceptual drawing illustrating orbit perturbations due to misaligned quadrupoles (**a**) or structures (**b**)

cillation is induced, due to the transverse wake field. The deflection caused by the wake field changes linearly with the beam displacement and with the bunch charge. In either case, the ensuing orbit is such that further emittance dilutions may result downstream of the perturbation due to the initial errors.

In this chapter we begin by reviewing beam-based alignment of single components. Such methods are particularly useful for those components with tight alignment tolerances, for example, near interaction regions. The techniques presented may be applied to the alignment of any accelerator component in general. For large accelerators, for which component-by-component alignment is too time-consuming or for which the beam trajectories must be routinely monitored, global orbit measurement and correction techniques are required. Many such algorithms will be presented in order of increasing complexity. So-called 'one-to-one' steering and R-matrix reconstruction are typically used not only to correct the orbit, but also to identify optical and/or instrumental errors. While such simple checks are absolutely mandatory, to achieve design beam parameters, more advanced tuning algorithms may be required. Common algorithms will be described including global beam-based alignment, singular value decomposition (SVD), application of wake field bumps, and dispersion-free steering.

3.1 Beam-Based Alignment

In many modern accelerators, the alignment tolerances on quadrupole and sextupole magnets are so tight that they cannot be achieved by state-of-the art surveying and installation methods. Typical residual alignment errors are in the range of 100–200 μm while the alignment tolerances may be even below 10 μm. The standard approach to meet and maintain tight tolerances is beam-based alignment.

Beam-based alignment determines the relative offset between magnet centers and nearby BPMs. If these offsets are sufficiently stable, a simple orbit correction (steering) can maintain a well-centered orbit until the optical alignment measurement is repeated at a later time (e.g., after several months).

3.1.1 Quadrupole Excitation

If the beam is not centered in a quadrupole magnet, and the strength of this quadrupole is varied, the beam receives a kick. This causes a change in the beam trajectory for single-turn measurements or a change in the closed orbit for measurements on a stored beam.

For a single-pass measurement, the dipole kick θ can easily be inferred by fitting the difference trajectory to a betatron oscillation including one additional kick at the location of the quadrupole. The dipole kick θ obtained from the fit is proportional to the quadrupole misalignment x_q and the change in the integrated quadrupole strength ΔK:

$$\theta = \Delta K \; x_q \,. \tag{3.2}$$

Note that the beam is offset from the center of the quadrupole by $-x_q$, so that there is no minus sign in (3.2) assuming $K > 0$ refers to a horizontally focusing quadrupole.

If beam-based alignment is performed using a stored beam, the additional kick of the closed orbit induced by the change in quadrupole strength is given by the sum of two components: the change in field strength and the change in the closed-orbit offset at the quadrupole. To lowest order [2],

$$\theta \approx \Delta K \; x_q - K \; \Delta x \,, \tag{3.3}$$

where x_q is the original quadrupole offset, Δx the change in closed-orbit position, K the integrated quadrupole gradient in units of m^{-1}, and a second-order term ($\Delta K \; \Delta x$) has been neglected. Applying the formula for the closed orbit distortion at the location of the dipole kick, (2.34), with $s = s_0$. Neglecting here the possible small contribution from the dispersion D_x, then

$$\Delta x = (\Delta K \; x_q - K \; \Delta x) \; \left(\frac{\beta}{2 \tan \pi Q} \right) \,, \tag{3.4}$$

which may be solved for Δx:

$$\Delta x = \Delta K \; x_q \left(\frac{\beta/(2 \tan \pi Q)}{1 + K\beta/(2 \tan \pi Q)} \right) \,. \tag{3.5}$$

Inserting this back into (3.3) gives the closed-orbit kick induced by a gradient change ΔK:

$$\theta = \Delta K \; x_q \left(\frac{1}{1 + K\beta/(2 \tan \pi Q)} \right) \,. \tag{3.6}$$

This is the stored-beam equivalent of (3.2).

The precision of this method is much improved by taking difference orbits for several quadrupole-to-beam off-sets, Δx_q, varied with a local bump [3]. One can also define a merit function

$$f(\Delta x_q) = \frac{1}{N_{\mathrm{BPM}}} \sum_{i=1}^{N_{\mathrm{BPM}}} \left[x_i(\Delta K) - x_i(-\Delta K) \right]^2 \,, \tag{3.7}$$

where N_{BPM} is the total number of BPMs in the ring and $x_i(\Delta K)$ are the BPM readings for a quadrupole strength change of ΔK. The quadrupole offset may then determined by minimizing $f(\Delta x_q)$ as a function of the bump amplitude Δx_q, using a least-squares parabolic fit. At the Advanced Light Source (ALS), this procedure allows determination of the center of the quadrupoles to within ± 5 μm [2] (in case of the ALS, the orbit at the quadrupole is varied with a single corrector and not by a closed bump).

This type of measurement does not require an independent power supply for each quadrupole to be aligned, but, for several magnets in series, a simple switchable shunt resistor across each magnet will suffice. Simultaneously, such shunt resistors allow a measurement of the local beta function, according to (2.28) or (2.29) of the previous chapter.

Figure 3.4 illustrates the application of this technique at the storage ring SPEAR. The left figure shows the circuit diagram for a magnet with shunt resistor, and the right figure presents a typical alignment measurement for a SPEAR quadrupole. Plotted in the right figure is the orbit shift induced by

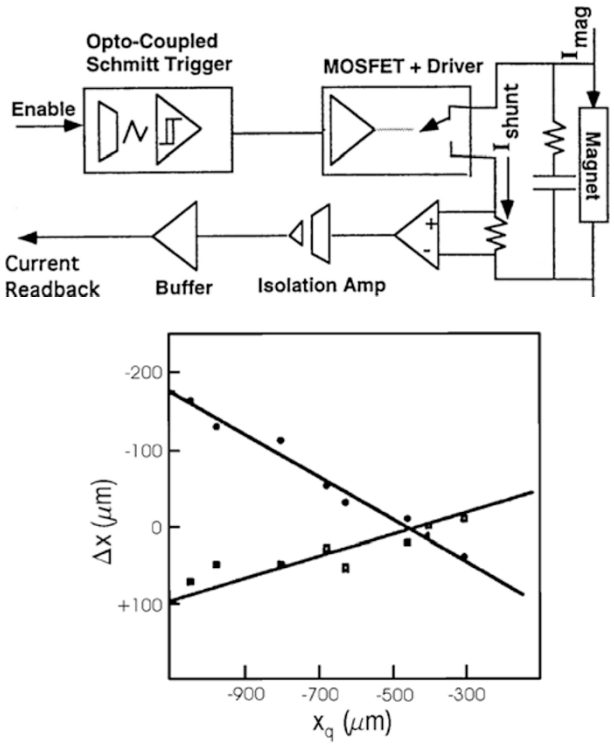

Fig. 3.4. Beam-based alignment with quadrupole shunts at SPEAR [4]: (*top*) electric circuit with shunt resistor; (*bottom*) shunt-induced orbit shift at two downstream BPMs as a function of the beam-position read back at the BPM nearest to the quadrupole being varied (Courtesy J. Corbett, 1998)

the shunt at two downstream BPMs as a function of the orbit at the shunted quadrupole, which is varied by a local bump. The orbit is centered in the quadrupole when no orbit shift is induced by the shunt (the intersection of the two lines).

If the number of BPMs is small and only groups of quadrupoles can be changed simultaneously, it is still possible to determine the quadrupole misalignments, by applying a statistical fit to a sufficiently large number of trajectories taken for different quadrupole-group excitations, different incoming conditions and different corrector settings. An interesting example of such an analysis can be found in [5].

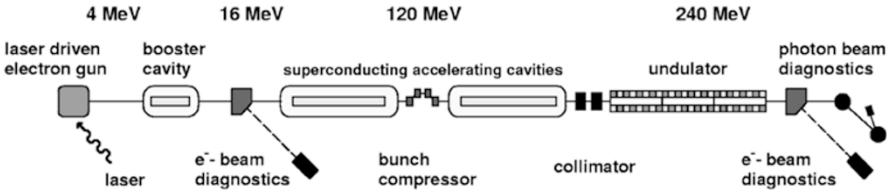

Fig. 3.5. Overview of the TTF linear accelerator including 2 accelerating modules (ACC1 and ACC2) and a bunch compressor chicane (BC2)

Another application of this method is illustrated for the Tesla Test Facility (TTF). An overview of part of the linear accelerator is shown in Fig. 3.5. In this measurement a horizontal corrector located just upstream of the bunch compressor chicane (BC2) was varied in steps for different settings of quadrupole settings. In the data shown in Fig. 3.6 the quadrupole of interest was the most upstream quadrupole in the triplet following the chicane. The next downstream beam position monitor was used for measurement of

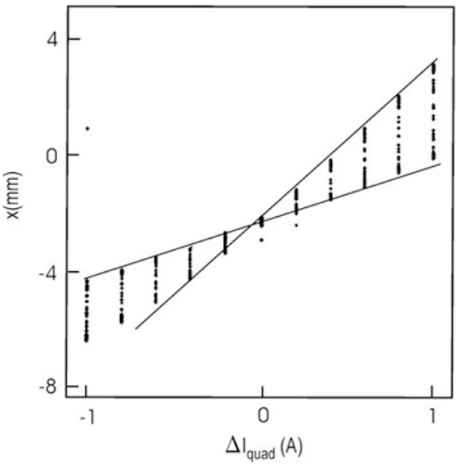

Fig. 3.6. Beam-based alignment of a single quadrupole at the TTF (Courtesy P. Castro, 2000)

the horizontal displacements. The orbit was centered when variation of the quadrupole field produced no change in the measured beam position (at the intersection of the lines).

3.1.2 Quadrupole Gradient Modulation

A scheme which allows continuous monitoring of quadrupole alignment and BPM offsets was implemented at LEP; see for example [6]. Here the strength of several quadrupoles was modulated at different frequencies in the range 0.8–15.6 Hz, and the induced oscillation amplitude, of the order of 1 μm was detected. Figure 3.7 shows the FFT over 4096 data points of this detector signal, at a time when four quadrupoles were modulated. Clearly visible are 4 peaks in the frequency sprectrum, corresponding to the four different modulation frequencies. The amplitude of the peak is proportional to the beam offset in that quadrupole.

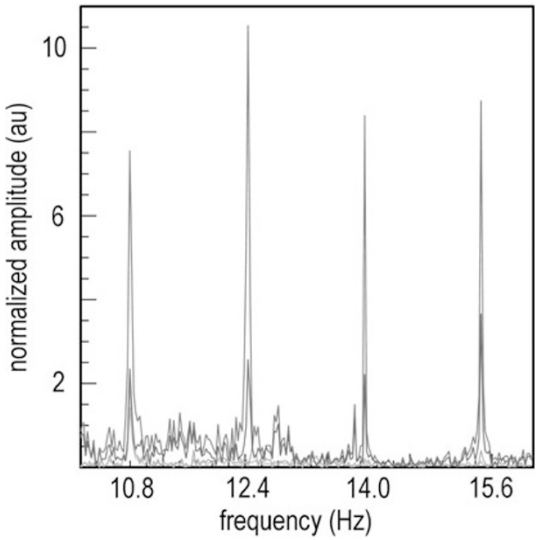

Fig. 3.7. FFT spectra with 4 modulated quadrupoles in LEP [6]. The amplitude of the peaks is proportional to the beam displacement in the 4 quadrupoles (Courtesy I. Reichel, 1998)

Using this 'K-modulation' technique, one could infer the BPM offsets from the naturally occurring beam-orbit jitter and orbit variation. This is illustrated in Fig. 3.8. The left figure shows a BPM orbit reading in LEP during several hours of a luminosity run. The reasons for the slow changes are not fully understood; the fast steps reflect corrections of the closed orbit. Making use of this natural orbit variation, one can plot the amplitude of the beam response to the quadrupole modulation as a function of the BPM

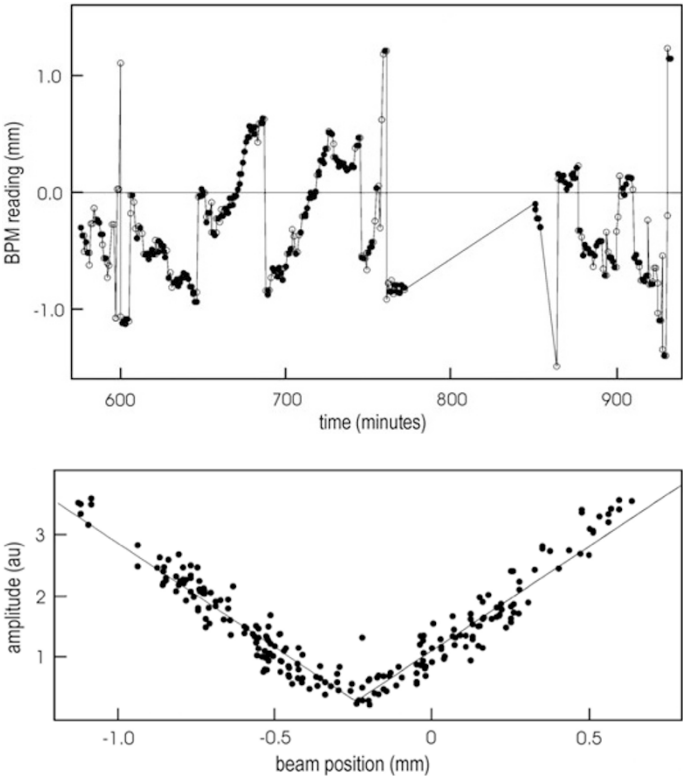

Fig. 3.8. Determination of BPM offsets using k modulation and natural orbit variation in LEP [6]: (*top*) natural orbit drifts and corrections during a LEP luminosity run at one quadrupole; (*bottom*) amplitude of beam response to k modulation vs. BPM orbit reading for the modulated quadrupole. The minimum of this plot gives the BPM offset. These data were taken continuously during 5 hours of luminosity run (Courtesy I. Reichel, 1998)

reading for the corresponding quadrupole. The result is a 'V plot', as shown in the right figure. The minimum in this plot determines the BPM reading at which the beam is centered in the quadrupole.

3.1.3 Sextupole Excitation

In present-day storage rings, it is often assumed that the sextupoles are well enough aligned with respect to the quadrupoles that only the quadrupole alignment has to be verified. An orbit off center in a sextupole will result in vertical dispersion, betatron coupling, or beta beating. Although, in principle, also the sextupoles in a storage ring can be aligned by changing their strength and measuring the induced orbit shift (which is a quadratic function of the excitation) there is little experience with such a scheme. To reach the same

sensitivity as for the equivalent quadrupole alignment, the change in the sextupole gradient ΔK_s would have to be equal to

$$\Delta K_s = \frac{\Delta K_q}{2x_s}\,, \tag{3.8}$$

where x_s is the horizontal orbit offset at the sextupole, and ΔK_q the corresponding change in quadrupole gradient. A different approach, which was tested at KEK [7], is to equip the sextupole magnets with additional quadrupole trim windings for beam-based alignment. This is based on the assumption that the magnetic centers of quadrupole trim coil and sextupole will coincide. Sextupole alignment with a precision better than 50 μm was demonstrated [7].

Local orbit bumps across single sextupoles have been used for the purpose of sextupole alignment at KEK [8, 9] and DESY [10]. The strengths of all sextupoles are changed together by ΔK_s and the induced orbit change is measured. Then the measurement is repeated for a different bump amplitude. The horizontal deflection depends quadratically on the horizontal bump amplitude, while the vertical deflection is a linear function:

$$\Delta\theta_x = -0.5\ \Delta K_s (x_{\mathrm{bump}} - x_s)^2\,, \tag{3.9}$$

$$\Delta\theta_y = \Delta K_s (x_{\mathrm{bump}} - x_s) y_s\,, \tag{3.10}$$

where x_{bump} is the amplitude of the bump, and x_s, y_s are the sextupole misalignments. The advantage of this method is that it does not require individual power supplies for the sextupoles.

The vertical sextupole alignment can be determined in a similar way, but in this case a (preferably large) horizontal orbit offset x_0 at the sextupole must first be introduced, to enhance the sensitivity. The vertical deflection angle then varies linearly with the amplitude of a vertical orbit bump at the sextupole as follows:

$$\Delta\theta_y = \Delta K_s (x_0 - x_s)(y_{\mathrm{bump}} - y_s)\,, \tag{3.11}$$

where we have also included a residual horizontal misalignment x_s. After measuring the vertical misalignment y_s, the original horizontal orbit can be restored.

Alternative approaches are conceivable: one could vary multiple sextupoles at once, and fit for multiple kicks. Also, one could vary the sextupole strength and measure the induced tune variation or the tune separation near the difference resonance [11].

In the final-focus systems of linear colliders, sextupole alignment is essential. At the SLC final focus, the orbit in the sextupoles was frequently measured and adjusted to maintain high luminosity. The SLC sextupole alignment procedure was based on varying the sextupole strength and detecting the induced optics (not orbit) change [12]. If the orbit is off center, the first order effect of the sextupole excitation is a waist shift (change in the beta function), skew coupling, or dispersion at the interaction point. These optics changes

can be quantified easily by reoptimizing the spot-size at the collision point, after a change in the sextupole strength. This reoptimization is done by scanning a group of quadrupole and skew quadrupole magnets excited together so that they only affect one optical parameter, e.g., either dispersion, skew coupling or waist shift. Such combinations of changes in magnet settings are called multiknobs; see the discussion in Chap. 2. For each setting of the multiknob, the IP spot size is remeasured with beam-beam deflection scans, and the magnets are finally set to the value for which the beam size is minimum. The change in the optimum settings of the multiknobs controlling waist, dispersion, etc., as a function of the sextupole excitation is proportional to the orbit offset at the sextupole. The measured offsets are corrected by means of closed bumps.

An interesting feature of the SLC final focus is that it comprises 2 pairs of interleaved sextupoles. The sextupoles in each pair, connected to the same power supply, are separated by an optical $-I$ transform. Thus, the alignment procedure actually consists in generating symmetric or antisymmetric orbit bumps for each sextupole pair, in response to the amount of waist motion or dispersion etc., induced by a change in the sextupole-pair strength [13].

3.1.4 Sextupole Movement

It is also possible to align the sextupole magnets by detecting the second-order effect of the sextupole excitation: the induced orbit kick. This method works well when the sextupoles are installed on precision movers, which can be used

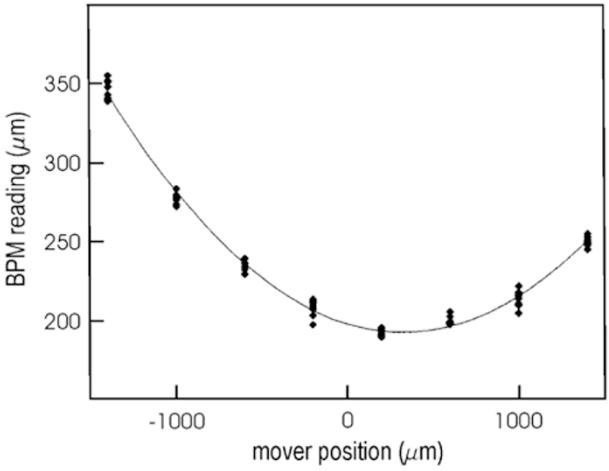

Fig. 3.9. Sextupole alignment in the Final Focus Test Beam (FFTB) [14]. The downstream orbit variation is measured as a function of sextupole mover position; the sextupole is aligned at the minimum of the parabola (Courtesy P. Tenenbaum, 1998)

for both the measurement and the alignment. The measurement principle is straightforward. Measuring the orbit change downstream as a function of horizontal or vertical sextupole-mover position results in a parabolic curve. The sextupole is aligned when the mover position is set to the minimum of this curve. A sample measurement from the FFTB [14] is displayed in Fig. 3.9.

3.1.5 Structure Alignment Using Beam-Induced Signals

For future high-gradient linear accelerators operating at even higher accelerating frequencies it becomes even more essential to center the beam orbit in the accelerating structures, thus minimizing the effect of transverse wake fields on the beam. Alignment techniques have been studied on test structures for the Next Linear Collider, which were installed in the SLAC linac as part of the ASSET experiment [15]. These studies demonstrated that the beam-induced dipole-mode signals can be used to center the beam to the level of 40 μm [16]. The result in Fig. 3.10 shows the amplitude and phase

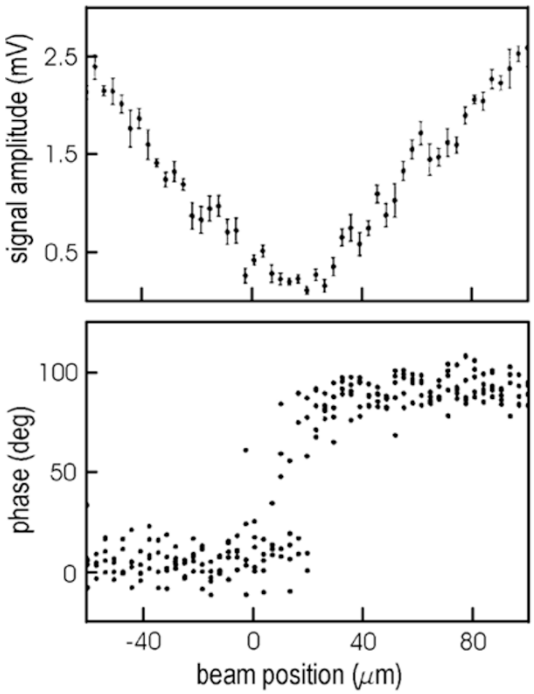

Fig. 3.10. Amplitude (*top*) and phase (*bottom*) of the beam-induced dipole mode signal in an X-band accelerating structure versus the nominal beam position (arbitrary zero), which was varied by steering correctors [16] (Courtesy M. Seidel, 1998)

(with respect to a reference phase derived from a BPM signal) of a 15-MHz wide slice of the beam-induced dipole mode signal, centered near 15 GHz, as a function of the nominal beam position. The beam position was varied with dipole steering magnets. Clearly visible is a minimum in the amplitude along with a 180 degree phase jump. Steering the beam to the position with minimum signal successfully centered the orbit in the structure as was verified by detecting the deflection experienced by a subsequent witness bunch.

We now turn our attention to global steering algorithms designed to efficiently align the beam relative to offset magnets and accelerating structures relying heavily on computational techniques. The algorithms are presented in order of increased complexity. Not by chance, this order coincides to a large degree with the order of implementation as an accelerator is being commissioned and the beam properties are refined.

3.2 One-to-One Steering

This algorithm aims to steer the beam so that the transverse displacements measured by beam position monitors (BPMs) are minimized. The BPMs are typically mounted near the center of quadrupoles since their sensitivity is highest at large β-function. A conceptual orbit steered one-to-one is shown in Fig. 3.11. The beam is successfully deflected to pass through the magnet center and, assuming that the BPM is not offset with respect to the quadrupole, the BPM would show zero displacement. Notice however that one-to-one steering generates dispersion will contribute to emittance dilutions.

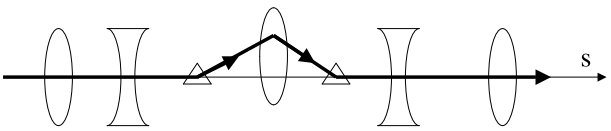

Fig. 3.11. Conceptual illustration of a closed bump that would minimize the BPM reading after one-to-one steering

In a transport line the beam centroid position measured downstream at location $s = j$ obeys

$$x_j = \sum_{i=0}^{j} \sqrt{\beta_i \beta_j}\theta_i \sin(\theta_j - \theta_i)\,, \tag{3.12}$$

which has contributions from each dipole kick θ_i and depends on the β-functions at the location of the initial disturbance (i) and at the observation point (j). The corrector magnet fields to be applied to minimize the BPM readings will be solved for assuming linear transport; that is, assuming that there are no nonlinear magnetic fields and that the measurements are made at low bunch current so that nonlinear wake field effects may be ignored.

In matrix form

$$\boldsymbol{x} = M\boldsymbol{\theta}\,, \tag{3.13}$$

where $\boldsymbol{x}$ is the set of measurements from m BPMs, $\boldsymbol{\theta}$ is the set of deflection angles to be applied by n correctors, and M contains the transfer matrix elements between the correctors and the BPMs:

$$x^t = (x_0, x_1, ..., x_m)\,, \tag{3.14}$$

$$\theta^t = (\theta_0, \theta_1, ..., \theta_n)\,, \tag{3.15}$$

$$M_{ij} = \sqrt{\beta_i \beta_j}\,\sin(\phi_j - \phi_i)\,. \tag{3.16}$$

Solving (3.13), the kick angles to be applied for minimizing the BPM readings are obtained:

$$M^t\boldsymbol{x} = M^t M\boldsymbol{\theta} \quad \text{or} \quad \boldsymbol{\theta} = (M^t M)^{-1} M^t \boldsymbol{x}\,. \tag{3.17}$$

If the number of correctors equals the number of BPMs, then M is a square matrix. In this case, (3.17) reduces to simply $\boldsymbol{\theta} = M^{-1}\boldsymbol{x}$. Otherwise the general form is taken. If $m > n$ the matrix is overdetermined. For $m < n$ the number of unknown corrector strengths exceeds the number of measurements, so that an independent measurement should be made after changing some parameter, for example, the beam energy. In a linear accelerator, (3.12) must be modified [17] to include the energy scaling factor $\sqrt{E_i/E_j}$, which reflects the transverse damping due to the longitudinal acceleration. This introduces n additional unknown variables, so that additional measurements are required to constrain the solution.

As motivation for the algorithms to be used below in the discussion of beam-based alignment and dispersion-free steering, the solution (3.17) can be equivalently formulated in terms of a minimization procedure, which is well adapted to computational evaluation. The function to be minimized, given by (3.13), is

$$\sum_j \Big[x_j - \sum_i M_{ji}\theta_i\Big]^2\,, \tag{3.18}$$

where x_j again represents the BPM measurements and the fitting function $\sum_i M_{ji}\theta_i$ contains the unknowns θ_i. The minimization procedure demands

$$\begin{aligned} 0 &= \frac{\partial}{\partial\theta_k}\Big[\sum_j (x_j - \sum_i M_{ji}\theta_i)^2\Big] \\ &= 2\sum_j \Big[x_j - \sum_i M_{ji}\theta_i\Big] M_{jk}\,, \end{aligned} \tag{3.19}$$

or

$$\sum_j M_{jk}x_j = \sum_j \sum_i M_{ji}M_{jk}\theta_i\,, \tag{3.20}$$

which is identical to (3.17).

One-to-one steering is used routinely during initial commissioning of an accelerator as it is by far the simplest of all steering algorithms. The procedure relies on having reasonably well functioning beam position monitors and may diverge in the presence of either large monitor errors or, possibly, with multiple smaller errors. A complementary algorithm, presented next, is useful to help identify BPM errors (polarity, gain, offset, etc.) and to help localize optical errors as well.

3.3 Lattice Diagnostics and R Matrix Reconstruction

Consider a beam line, without any elements coupling horizontal and vertical motion, as shown in Fig. 3.12 consisting of dipole and quadrupole magnets, BPMs and corrector magnet dipoles. The point-to-point transfer map between any two points (1) and (2) is given by

$$\begin{pmatrix} x \\ x' \end{pmatrix}_2 = \begin{pmatrix} R_{11} & R_{12} \\ R_{21} & R_{22} \end{pmatrix} \begin{pmatrix} x \\ x' \end{pmatrix}_1 . \tag{3.21}$$

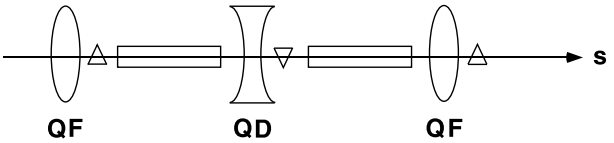

Fig. 3.12. Simple FODO lattice. Shown are the focussing quadrupoles (QF), the defocussing quadrupoles (QD), and dipoles (rectangles). The BPMs are usually mounted within the quadrupoles. Corrector magnets are denoted by triangles

Let the initial point (1) be at a corrector and the final point (2) be at a BPM. Two measurements are required to determine R_{12}: x_{BPM} with the nominal beam trajectory and the nominal initial values $(x, x')_{\mathrm{COR}}$, and with x_{BPM} for the initial position and slope $(x, x' + \theta)_{\mathrm{COR}}$, i.e., after the beam is kicked by an angle θ. The difference in x_{BPM} between these two measurements is $R_{12} = \Delta x/\theta$. In practice to decrease sensitivity to measurement error, one introduces a series of large betatron oscillations by varying the corrector in steps. The response of the BPM readings to these perturbations [18] is then measured. The resulting dependence of position on the kick angle θ is fitted with a straight line as shown in Fig. 3.13.

Shown in Fig. 3.14 is an example of a beam trajectory after excitation by a corrector magnet and an amplitude fit using many downstream BPMs. For good viewing conditions the measured trajectory is plotted for the case of a maximum kick angle $\theta = \theta_{max}$. The solid line connects the measurements from each BPM. The dashed line represents the fitted positions $x_i = R_{12}^{\theta \to i}\theta + x_{o,i}$ evaluated at θ_{max} where $x_{o,i}$ is an offset at the ith BPM.

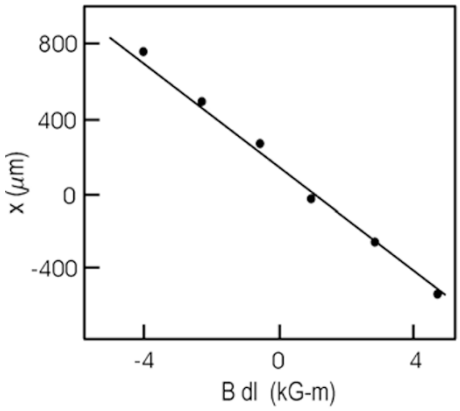

Fig. 3.13. Example of an R_{12} measurement: transverse position x versus $\int B\ \mathrm{d}l$, where the kick angle, in terms of the magnetic rigidity $B\rho$, is $\theta = \int B\ \mathrm{d}l/(B\rho)$

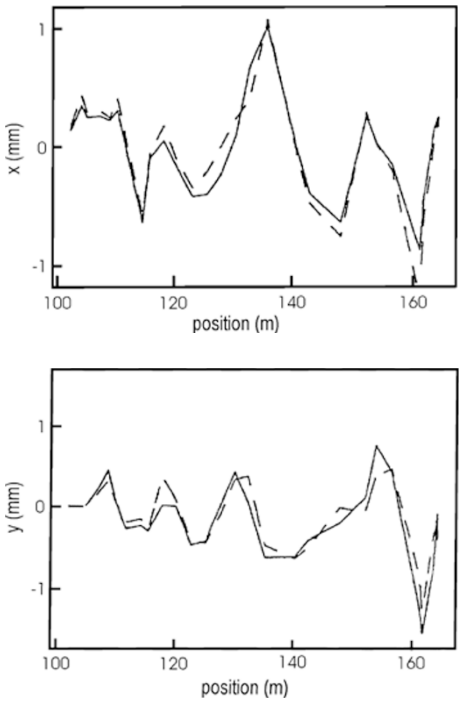

Fig. 3.14. Comparison of measured data (*solid curve*) and amplitude fit (*dashed curve*). Plotted are the horizontal and vertical beam positions as measured as a function of distance along the transport line. See also [19]

in the linear fit. A single value of θ and the values of m BPM offsets $x_{o,i}$ are fitted, so as to minimize the difference between the measured BPM readings and the model prediction, i.e., $\sum_i (x_{\mathrm{BPM},i} - R_{12}^{\theta\to i}\theta - x_{o,i})^2$. Here $R_{12}^{\theta\to i}$ is the (1,2) transport-matrix element between the corrector and the ith BPM computed by the optics model. To probe all magnetic elements in the beamline, a second measurement is required using a second corrector dipole separated by about 90° in betatron phase advance. Discrepancies between the meas-

urement, $x_{\mathrm{BPM},i}$ and the fit, x_i, are used to reveal phase errors, which could result from a shorted quadrupole magnet, and/or "bad" BPMs for example. Identification and exclusion of bad BPMs is required for good convergence of steering algorithms.

Assuming the linear transport matrices between the different correctors and the transport matrices between adjacent BPMs are known with sufficient accuracy, the R matrix between the correctors and the BPMs can be determined by a simple least squares fit [18]. Including the additional constraint that the R matrix has to be symplectic eliminates several degrees of freedom, but then the problem must be solved by non-linear regression [18]. Reference [18] describes how a rigorous error analysis allows an estimate of the unknown systematic errors.

Suppose the agreement between the measured data and fit is unsatisfactory. In the absence of hardware errors, this may result from systematic measurement errors or from an incomplete model. Accuracy of the model is vital for basic optics checkout and requires, for example, accurate representations of magnetic field strengths.

In a linear accelerator, it may be necessary to take into account the energy dependence of the point-to-point transfer matrix elements. The change in the betatron phase $\Delta\psi$ relative to the expected phase ψ is given by

$$\frac{\Delta\psi}{\psi} = \delta\xi\,, \tag{3.22}$$

where δ is the relative energy deviation and ξ is the chromaticity (in a storage ring ξ is related to Q' via $\xi \equiv Q'/Q$, where Q denotes the betatron tune). With $\xi = -1/\pi$ for a 90° FODO cell, then a 1% energy error corresponds to a change in phase advance of $\Delta\psi = -0.003\psi$ per cell.

To take into account the energy dependence of the transport matrix, the matrix elements may be expanded in a Taylor series. Keeping the linear term only, the transport matrix from the entrance ('1') to the end of the ('2') of the linac can be written as

$$\begin{pmatrix} x \\ x' \end{pmatrix}_2 = \prod_{k=1}^{N_s} \begin{pmatrix} R_{1,1_k} + \frac{\mathrm{d}R_{1,1_k}}{\mathrm{d}E_k}\Delta E_k & R_{1,2_k} + \frac{\mathrm{d}R_{1,2_k}}{\mathrm{d}E_k}\Delta E_k \\ R_{2,1_k} + \frac{\mathrm{d}R_{2,1_k}}{\mathrm{d}E_k}\Delta E_k & R_{2,2_k} + \frac{\mathrm{d}R_{2,2_k}}{\mathrm{d}E_k}\Delta E_k \end{pmatrix} \begin{pmatrix} x_0 \\ x'_0 \end{pmatrix}_1 , \tag{3.23}$$

where N_s is the number of regions ('sectors', typically taken to be one sector per power source) into which the accelerator has been subdivided, and the total R matrix is expressed as a product of the R matrices for the different sectors. A possible procedure now consists of

1. measuring the transverse position x_m after the beam has been deflected,
2. selecting a set of E_k's,
3. comparing the measured position x_m with the expected, or calculated, position x_c by computing

$$\chi^2 = \sum (x_m - x_c)^2 \,, \tag{3.24}$$

where the sum is over all the BPMs used in the measurement, and

4. iterating steps 2 and 3 to minimize the χ^2.

An example of this approach is shown in Fig. 3.15 for the SLAC linear accelerator [20]. In the top plot an amplitude fit was used without taking into account any energy deviations (as in Fig. 3.14). In the bottom plot, also the values of E_k were fitted. The minimum χ^2 corresponded to an energy error of about 30%, which far exceeded the estimated uncertainty in the energy. Possible reasons for the discrepancy might include calibration errors of the quadrupole strengths, random errors in the BPM gains, or wake fields, which all are not included in the model. Nonetheless, the dynamics were made more predictable by incorporating the fitted energy errors into the accelerator model, despite the fact that the actual source of the error (perhaps wake fields) was different from the assumed one (energy errors).

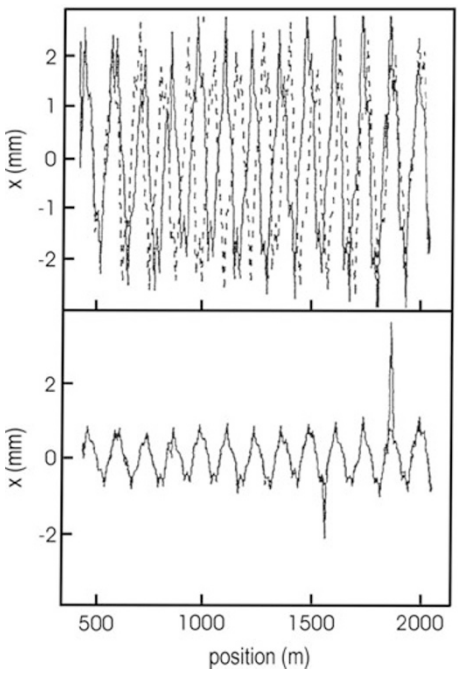

Fig. 3.15. Comparison of measured data and fit to betatron amplitude only (*top*) or fit to both betatron amplitude and energy in the different linac sections (*bottom*). Plotted is the horizontal beam position as a function of distance along the linear accelerator (Courtesy T. Himel, 1999)

3.4 Global Beam-Based Steering

We next present a more global approach to beam-based alignment than that discussed previously. We consider beam-based steering algorithms as ones

which provide information on magnet, BPM, or structure misalignments using measurements with the beam. With this definition, one-to-one steering may also be considered a beam-based alignment algorithm since the applied kicks θ are related to the quadrupole (or BPM) displacements Δx by $\theta = K\Delta x$, where K is the integrated quadrupole focussing field.

More generally, we take in this example into account that the electrical zero of the BPMs may not be coincident with the magnetic center of the quadrupoles and that the quadrupoles themselves may be displaced with respect to the reference axis. The coordinate system used is sketched in Fig. 3.16. Here the beam position x measured with respect to some reference axis, which is common to all magnets, is given as a sum of the quadrupole displacement x_q, the difference in location of the electrical center of the BPM and the magnetic center of the quadrupole x_{bpm}, and the measured BPM value x_m.

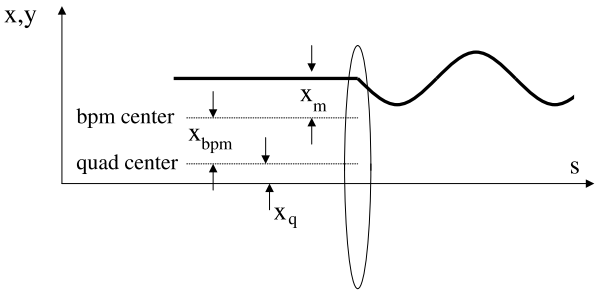

Fig. 3.16. Coordinate system used in the example of beam-based alignment (Courtesy C. Adolphsen, 2000)

The beam position x_k and angle $x_k{}'$ at quadrupole k, defined with respect to the reference axis, are given by [21]

$$\begin{pmatrix} x_k \\ x_k{}' \\ 1 \end{pmatrix} = \sum_{j=1}^{k-1} R_{j+1,k} \left\{ R_{j,j+1} \left[\begin{pmatrix} x \\ x' \\ 1 \end{pmatrix}_j + \begin{pmatrix} -x_{q,j} \\ 0 \\ 0 \end{pmatrix} \right] + \begin{pmatrix} x_{q,j} \\ 0 \\ 0 \end{pmatrix} \right\} , \tag{3.25}$$

where $()_j$ gives the beam position and angle with respect to the quad center, the term in [] is the beam position with respect to the reference axis, $R_{j,j+1}[]$ is the beam position with respect to the reference axis transported between quad j and quad $j+1$, and the term in {} is the beam position and angle with respect to the quad center transported between quads j and $j+1$. Rearranging terms gives

$$\begin{pmatrix} x_k \\ x_k{}' \\ 1 \end{pmatrix} = R_{0,k} \begin{pmatrix} x \\ x' \\ 1 \end{pmatrix}_0 + \sum_{j=1}^{k-1} (R_{j+1,k} - R_{j,k}) \begin{pmatrix} x_{q,j} \\ 0 \\ 0 \end{pmatrix} , \tag{3.26}$$

where the sum is taken over upstream quadrupoles. The function to be minimized is then

$$\sum_k \Big[x_m - (x_k - x_q - x_{\mathrm{bpm}}) \Big]^2 , \tag{3.27}$$

where x_m are the measurements and $(x_k - x_q - x_{\mathrm{bpm}})$ is the fitting function with unknowns x_q, x_{bpm} and the initial position and angle x_0 and x_0'.

The number of measurements is about half the number of unknowns. So the system is underconstrained. To constrain the solution, two independent measurements are required. An independent set of data may be obtained by scaling all the quadrupoles and correctors by a common factor and repeating the measurements. Multiple such scalings may be used to overdetermine the system which reduces the sensitivity of the solution to statistical errors.

3.5 Singular Value Decomposition

A common situation is that the BPM offsets are known fairly well and the orbit already fulfills a number of constraints, but many of the corrector magnets are strongly excited with some of them 'fighting' (compensating) each other. Fortunately, there exists a very powerful technique to reduce the rms strength of the orbit correctors, while maintaining a set of constraints. This technique is sometimes called 'corrector ironing' [22] and it is based on the 'singular value decomposition' (SVD) [23].

The linear equation to be solved is

$$\Delta\mathbf{x} = \mathbf{A} \cdot \theta \,, \tag{3.28}$$

where the vector $\Delta\mathbf{x} = (\Delta x_1, \ldots \Delta x_m)$ may describe the desired correction (or constraint) at m BPMs, and $\theta = (\theta_1, \ldots, \theta_n)$ are the excitation strengths of n correctors, that we want to determine. If $m \geq n$, we can decompose the matrix $\mathbf{A}$ as

$$\mathbf{A} = \mathbf{U} \cdot \begin{pmatrix} w_1 & 0 & \ldots & 0 \\ 0 & w_2 & \ldots & 0 \\ & \ldots & \ldots & \\ 0 & 0 & \ldots & w_n \end{pmatrix} \cdot \mathbf{V}^t \,. \tag{3.29}$$

The column vectors of the $m \times n$ matrix $\mathbf{U}$ and the $n \times n$ matrix $\mathbf{V}$ are orthonormal,

$$\mathbf{U}^t \cdot \mathbf{U} = \mathbf{I}_n \,, \tag{3.30}$$

$$\mathbf{V}^t \cdot \mathbf{V} = \mathbf{I}_n \,, \tag{3.31}$$

where $\mathbf{I}_n$ denotes the $n \times n$ unity matrix. The decomposition of (3.29) can be performed, for example, using the FORTRAN subroutine described in [23]. An SVD decomposition is also provided in a convenient form by many mathematical analysis packages, such as MATLAB [24].

We now consider three different cases: First, we suppose the number of correctors is equal to the number of BPMs. In this case the matrix $\mathbf{A}$ is square. The formal solution is given by

$$\theta = \mathbf{A}^{-1} \cdot \Delta\mathbf{x} = \mathbf{V} \cdot \begin{pmatrix} 1/w_1 & 0 & \dots & 0 \\ 0 & 1/w_2 & \dots & 0 \\ & \dots & \dots & \\ 0 & 0 & \dots & 1/w_n \end{pmatrix} \cdot \mathbf{U}^t \cdot \Delta\mathbf{x}\,. \tag{3.32}$$

If none of the w_i is zero, this is the unique solution to the problem. If one or more of the w_i are zero, the equation may not have an exact solution, but for these w_i one can simply replace $1/w_i$ by 0, and with this replacement (3.32) still gives the solution in a least squares sense. This means it minimizes the distance $r = |\mathbf{A}\cdot\theta - \Delta\mathbf{x}|$. Furthermore, the solution vector θ so obtained is the (either least-squares or exact) solution with the smallest possible length $|\theta|^2$. In other words, the solution derived from the SVD decomposition also minimizes the rms strength of the correctors.

In addition, it is worthwhile to note that the columns of $\mathbf{U}$ whose same numbered w_i are nonzero form an orthonormal set of basis vectors that span the range of the matrix $\mathbf{A}$ while the columns of $\mathbf{V}$ whose same-numbered elements w_j are zero form an orthonormal set for the nullspace of $\mathbf{A}$.

Next, we consider the case that there are fewer equations than correctors. In this case, we can simply add rows with zeroes to the vectors and matrices of (3.28) until the matrix is square, and then apply the SVD formalism, as described above. In this case, there is (at least) one zero eigenvalue w_j for every row of zeroes added.

Finally, in the case of more BPM constraints than unknown correctors ($m > n$), SVD works just as well. In general the w_j will not be zero, and the SVD solution will agree with the result of a least-square fit. If there are still some small values w_j, these indicate a degeneracy in $\mathbf{A}$ and the corresponding $1/w_j$ should be set to zero as before. The corresponding column in $\mathbf{V}$ deserves attention, since it describes a linear combination of corrector excitations, which does not affect the constraints.

The SVD steering algorithm has been used successfully at many accelerators, for example, at the synchrotron light source SPEAR [25], throughout the SLC, and most recently at LEP. Applications include not only the minimization of corrector strengths and the identification of strongly excited correctors 'fighting' each other, but also orbit feedback, dispersion-free steering, and the computation of optical tuning knobs, e.g., for the beta function, dispersion, or coupling. Multiknobs were discussed in Sect. 2.5.

An Example of SVD. As a more concrete illustration, let us consider two steering correctors, separated by a betatron phase advance of π, which are followed by two BPMs at locations 1 and 2, which are also a phase of π apart from each other.

After applying a convenient normalization, the matrix equation relating the corrector strengths θ_1 and θ_2 with the BPM readings x_1 and x_2 is

$$\begin{pmatrix} x_1 \\ x_2 \end{pmatrix} = \begin{pmatrix} 1 & -1 \\ -1 & 1 \end{pmatrix} \begin{pmatrix} \theta_1 \\ \theta_2 \end{pmatrix} . \tag{3.33}$$

The 2×2 matrix $\mathbf{A}$ can be decomposed as follows:

$$\mathbf{A} \equiv \begin{pmatrix} 1 & -1 \\ -1 & 1 \end{pmatrix} \tag{3.34}$$

$$= \begin{pmatrix} \frac{1}{\sqrt{2}} & \frac{1}{\sqrt{2}} \\ -\frac{1}{\sqrt{2}} & \frac{1}{\sqrt{2}} \end{pmatrix} \begin{pmatrix} 2 & 0 \\ 0 & 0 \end{pmatrix} \begin{pmatrix} \frac{1}{\sqrt{2}} & -\frac{1}{\sqrt{2}} \\ \frac{1}{\sqrt{2}} & \frac{1}{\sqrt{2}} \end{pmatrix} \tag{3.35}$$

$$\equiv \mathbf{U}\mathbf{W}\mathbf{V}^t , \tag{3.36}$$

where W denotes the diagonal matrix. Suppose now we want to steer to $x_{t,1} = 1$ and $x_{t,2} = 0$. An exact solution does not exist, since there is no corrector between the two BPMs and the latter are a phase advance of π apart. However, there is an SVD solution:

$$\begin{pmatrix} \theta_1 \\ \theta_2 \end{pmatrix} = \mathbf{V}\mathbf{W}^{-1}\mathbf{U}^t \begin{pmatrix} 1 \\ 0 \end{pmatrix} \tag{3.37}$$

$$= \begin{pmatrix} \frac{1}{\sqrt{2}} & \frac{1}{\sqrt{2}} \\ -\frac{1}{\sqrt{2}} & \frac{1}{\sqrt{2}} \end{pmatrix} \begin{pmatrix} \frac{1}{2} & 0 \\ 0 & 0 \end{pmatrix} \begin{pmatrix} \frac{1}{\sqrt{2}} & -\frac{1}{\sqrt{2}} \\ \frac{1}{\sqrt{2}} & \frac{1}{\sqrt{2}} \end{pmatrix} = \begin{pmatrix} \frac{1}{4} \\ -\frac{1}{4} \end{pmatrix} . \tag{3.38}$$

Hence, the SVD solution equals $\theta_1 = 1/4$ and $\theta_2 = -1/4$. For these corrector settings one obtains the BPM readings $x_1 = 1/2$ and $x_2 = -1/2$, where indeed the quadratic distance to the target values, $\sum_i (x_{t,i} - x_i)^2$, assumes a minimum. Not only does SVD determine a pair of corrector settings for which the BPM readings are closest to the solution looked for, but in addition, among all possible such solutions (adding any constant to the above values of θ_1 and θ_2 would give the same minimum value of $\sum_i (x_{t,i} - x_i)^2$), it finds that one which also minimizes the corrector strengths, namely the sum of the squares $\sum \theta_i^2$.

3.6 'Wake Field Bumps'

Through the early 1990's emittance dilutions in the SLC linac were controlled by imposing tight tolerances on injection errors as a precursor to BNS damping [26, 27], steering using both one-to-one correction and localized beam-based alignment [21, 28], and by invoking BNS damping. The name BNS damping refers to V. Balakin, A. Novokhatsky, and V. Smirnov, who in the early 1980s proposed this type of scheme, in which the tail of the bunch is focussed more weakly than the bunch head in order to compensate

for the defocusing effect of the single-bunch wake field [29]. At the SLC the variation of focusing across the bunch was achieved by introducing an energy difference. More details will be discussed in Chap. 4.

As the beam currents were increased, a more localized emittance preservation technique was developed in which empirically determined trajectory oscillations ('bumps') were used to cancel emittance dilutions from transverse wake fields and dispersive errors. While the origins of the disturbances could not be easily localized longitudinally along the linac, the accumulated effects could be cancelled using such bumps and the emittance dilution could be reduced by a factor of almost ten [30]. The effect on the beam was determined by emittance measurements near the end of the linac.

Two trajectories in both x and y are shown [30] in Fig. 3.17. Both trajectories produced about the same small emittance measured near the end of the linac. Notice the vertical scale which shows excursions of nearly 750 μm peak-to-peak. While wake field bumps were used for many years, it became clear as the currents were increased that this technique was inherently unstable; small (e.g., thermal) changes in the reference line phase, for example, changed the phase advance over the bump range so that even this more localized correction scheme was not sufficiently local to be stable against realistic variations in the accelerator. Both trajectories in Fig. 3.17 resulted in about the same

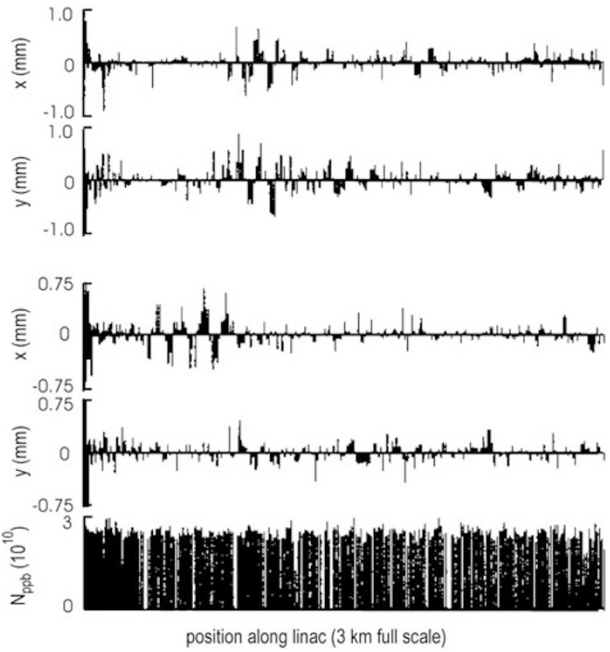

Fig. 3.17. Two measured orbits with empirically determined coherent betatron oscillations used to cancel accumulated wake field and dispersion errors (Courtesy J. Seeman, 2000)

final beam emittances indicating that the procedure did not converge to a unique solution.

Physical insights were gained by simulations carried out using the program LIAR [31]. The model included representative amplitudes of the wake field bumps which minimized the relative emittance growth at the locations of the measurements. The simulated relative growth in normalized emittance [32, 33] is shown in Fig. 3.18 as a function of position along the linac. Several important conclusions were drawn from this and other simulation results:

- At the first emittance measurement, the optimization had been made in a location where the energy spread of the beam was large; that is, a compromise was made using wake field bumps between correction of dispersive and wake field-induced errors.
- Between the emittance measurement stations, there was uncontrolled emittance growth.
- Between the final emittance measurement station and extraction of the beam from the linac, there was significant emittance growth.
- Most importantly, being nonlocal in nature, small changes in the phase advance could destroy this delicate cancellation. In practice this caused significant time-dependent variations in the measured emittances [34, 35, 36, 37].

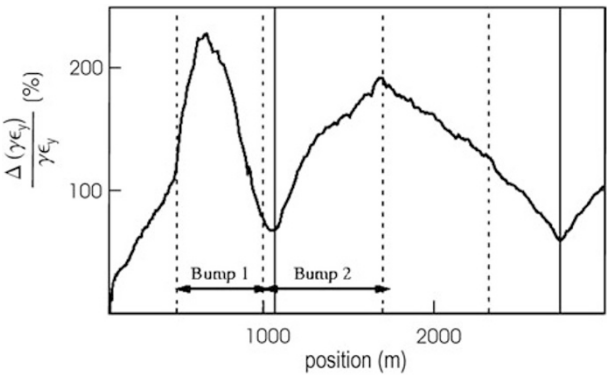

Fig. 3.18. Simulated emittance growth as a function of position along the linac. The locations of the feedback loops, which controlled the amplitude of the wake field bumps, are shown along with the locations of the emittance measurements (Courtesy R. Assmann, 2000)

3.7 Dispersion-Free Steering

So far we have described *one-to-one steering* which is a first step in orbit optimization but is imperfect as minimization of the BPM reading in a displaced quadrupole generates dispersive errors, *beam-based alignment* of quadrupole

displacements which works beautifully at low beam currents where there is no wake field-generated dispersion, and wake field bumps which while more local than BNS damping is highly sensitive to small perturbations in the electromagnetic optics. With perfect implementation of either procedure, dispersive emittance dilutions may still result. As an example, consider a closed trajectory bump of the kind illustrated in Fig. 3.3. It has been shown [38] using LIAR and realistic optical parameters of the SLC linac that a closed 100 μm π-bump at a quadrupole located early in the linac generates nearly 0.5 mm dispersion at the end of the linac. Naively, about 6 such bumps acting independently would produce a dispersive emittance contribution equal to the final emittances typically achieved at the SLC.

Dispersion-free steering [35, 36, 38] is an algorithm which corrects even more locally the dispersive errors from misaligned quadrupoles *and* the dispersive errors arising from transverse wake fields. For mostly technical reasons (e.g., data acquisition and processing time) implementation was unduly delayed at the SLC. Dispersion-free steering (and rf phase stability [39, 40, 41]) proved crucial for maintaining stable linac emittances at the SLC.

The centroid trajectory[1] is given by

$$x_j = \sum_{i=1}^{j-1} \sqrt{\frac{E_i}{E_j}} \sqrt{\beta_i \beta_j}\, \theta_i \sin(\phi_j - \phi_i) \tag{3.39}$$

$$= \sum_{i=1}^{j-1} R_{12}^{ij} \theta_i \,, \tag{3.40}$$

where the damping factor $\sqrt{E_i/E_j}$ has been included. To constrain the system, one can equivalently change the beam energy (which may be difficult in practice) or scale the strength of the lattice, i.e., the strengths of the quadrupoles. Then the orbit difference is measured for a deflection applied in the original lattice and in the scaled lattice. This orbit difference amounts to

$$\Delta x_j \approx \sum_{i=1}^{j-1} \Big[R_{12}^{ij} - \sqrt{\frac{E_i}{E_j}} \sqrt{\beta_{i,\kappa} \beta_{j,\kappa}} \sin(\phi_{j,\kappa} - \phi_{i,\kappa}) \Big] \theta_i$$

$$= \sum_{i=1}^{j-1} R_{12,\kappa}^{ij} \theta_i \,, \tag{3.41}$$

where $\beta_{i,\kappa}$ and $\phi_{i,\kappa}$ denote the beta function and betatron phase in the scaled lattice, and the change in lattice focussing is expressed by the parameter

$$\kappa = \frac{\Delta K}{K} + 1 \,, \tag{3.42}$$

where K is the quadrupole strength.

[1] a warning: intrabunch position-energy correlations, when projected, may result in measured centroid displacements which underestimate the contributions from off-axis bunch tails

The function to be minimized is

$$\sum_j \Big[x_j - \sum_i M_{ji}\theta_i\Big]^2 , \tag{3.43}$$

where x_j is an $m \times 1$ vector containing the difference measurements and the fitting function is given by $\sum_i M_{ji}\theta_i$ where θ_i is an $n \times 1$ vector of unknowns. In the simplest case, the coefficients M_{ji} represent an $m \times n$ matrix containing the transfer matrix elements $M_{ji} = R_{12}^{ij}$.

In practice it is not difficult to minimize not only the absolute orbit, but simultaneously several (k) difference orbits Δx. In this case x_j is a $(k+1) \times 1$ vector containing the difference measurements and the absolute orbit, M_{ji} is a $(k+1) \times n$ matrix and θ remains an $n \times 1$ matrix. This approach was used at the SLC where in addition, to overconstrain the solution and minimize systematic errors arising from magnet hysteresis, the measurements were performed for $k = 4$ or 5 values of κ corresponding to energy variations of $+5\%$ to -30%. In later years, the problem of magnet hysteresis was eliminated and the application became noninvasive as two independent measurements could be obtained *without* changing the lattice by measuring independently the orbits of the electrons and positrons which passed through the same lattice. The opposite charge of electrons and positrons was equivalent to a lattice scaling by -200%.

Shown in Fig. 3.19 are absolute ($\kappa = 1.0$) and difference trajectories ($\kappa = 0.9$, 0.8, and 0.7) measured after trajectory steering of the SLC linac [38] using 20-pulse BPM averaging. With an equivalent energy change of 30% ($\kappa = 0.7$), a difference trajectory of up to 1.5 mm was observed. Similar measurements made after iteration of dispersion-free steering [38] are given in Fig. 3.20. Iteration proved useful to reduce sensitivity to errors in the

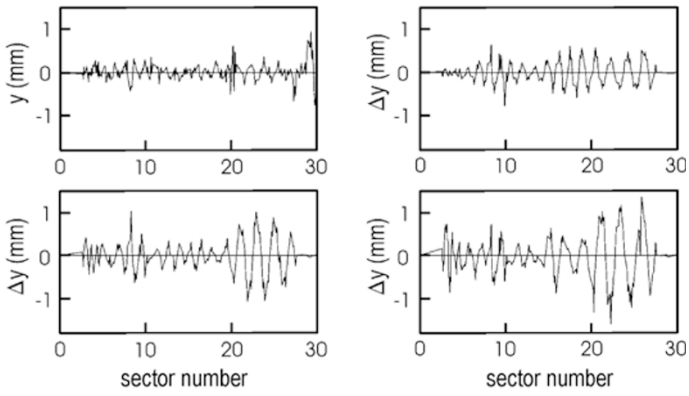

Fig. 3.19. Absolute and difference vertical trajectories measured after trajectory steering before dispersion-free steering of the SLC linac (Courtesy R. Assmann, 2000)

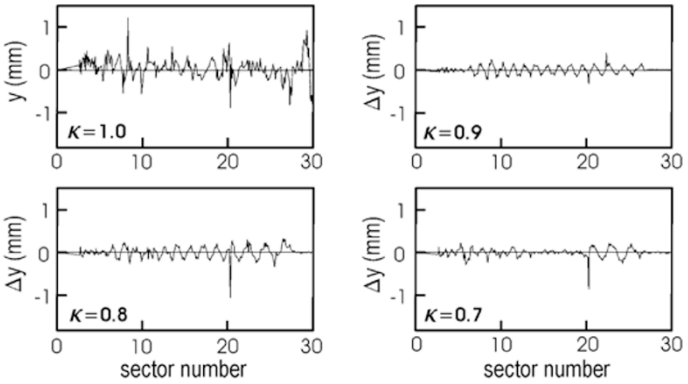

Fig. 3.20. Absolute and difference vertical trajectories measured after dispersion-free steering in the SLC linac (Courtesy R. Assmann, 2000)

assumed optics even though experience showed that the first iteration yielded the largest improvements. With $\kappa = 0.3$, neglecting the errant point due possibly to a bad BPM near sector 20, the maximum orbit difference after dispersion-free steering was reduced from 1.5 mm to less than 200 μm. Notice that the rms of the measurements of the absolute orbit are actually larger following dispersion-free steering. This suggests that significant BPM and/or quadrupole misalignment errors were still present.

3.8 Errors

For simplicity of expression, measurement errors have been neglected up to now. At the SLC, error sources and their typical rms contributions included BPM resolution errors $\sigma(x_j) < 10$ μm, BPM misalignments $\sigma_{\rm bpm} \sim 100$ μm, and systematic errors arising from beam jitter and/or slow drifts $\sigma_{\rm sys} \sim 20$ μm. To propagate the measurement errors used in the minimization procedures, a weighting function may be defined as

$$w_j = \frac{1}{\sum_j {\sigma_{m,j}}^2}\,, \tag{3.44}$$

where the subscripts m give the different error sources and j is a sum over the BPM measurements. The functions to be minimized then are (c.f. (3.18), (3.27), and (3.43))

$$\sum_j \left[\frac{x_j - \sum_i M_{ij}\theta_i}{\sum_m {\sigma_{m,j}}^2}\right]^2 \quad \text{(one-to-one steering)}\,,$$

$$\sum_k \left[\frac{x_m - (x_k - x_q - x_{\rm bpm})}{\sum_m {\sigma_{m,j}}^2}\right]^2 \quad \text{(beam-based alignment)}\,,$$

$$\sum_j \quad \left[\frac{x_j - \sum_i M_{ij}\theta_i}{\sum_m {\sigma_{m,j}}^2}\right]^2 \qquad (\text{dispersion}-\text{free steering})\,. \tag{3.45}$$

A goodness of fit parameter, or $\chi-$squared may be correspondingly constructed. In the dispersion-free steering example given above for which both the trajectory and the trajectory differences were to be simultaneously minimized,

$$\chi^2 = \sum_j \left[\frac{{x_j}^2}{{\sigma_{\rm bpm}}^2} + \sum_\kappa \frac{{\Delta x_{j,\kappa}}^2}{{\sigma_{\rm sys}}^2}\right]\,, \tag{3.46}$$

where the second summation over κ corresponds to the difference orbits for the different energy scalings under which the measurements were made. The errors from BPM resolution were assumed to be negligible and the summation over errors has been simplified to reflect the dominating errors; that is, the systematic errors contribute less than the alignment errors in the measurements of the absolute trajectories, while in the measurements of difference trajectories the BPM misalignments cancel and the associated errors are therefore set to zero.

3.9 Orbit Feedback

Automated feedback systems that continually stabilize the beam orbit are becoming more common in accelerators. A comprehensive overview of orbit feedback system design can be found in [42]. A simple orbit feedback maintains a constant orbit by adjusting the strength of 2 or 4 steering correctors based on BPM readings. Many orbit feedback systems employ an SVD algorithm which flattens the orbit while at the same time minimizing the strength of the correctors.

Slightly more complicated feedback loops are designed so that they maintain both the beam orbit and the beam energy. Orbit and energy can be separated using BPMs at dispersive locations. The orbit is corrected via steering correctors; the beam energy by adjustments to some upstream rf phase.

The effectiveness of a feedback can be tested by measuring its response to a step change. An example in Fig. 3.21 shows the response of an SLC feedback loop to a sudden step change in energy. The picture illustrates the improvement achieved by increasing the number of feedback BPMs to better constrain the fit. Specifically, 2 BPMs separated by $-I$ were included so that the sum of the (difference) signals from the two BPMs gave the dispersive contribution to the particle orbit independent of the betatron component. In addition to having a well understood accelerator model, for accelerators with high repetition frequency (with intra-pulse spacing comparable to the the response time of the correction magnets) it was found necessary to carefully match the response times of correction magnets [43].

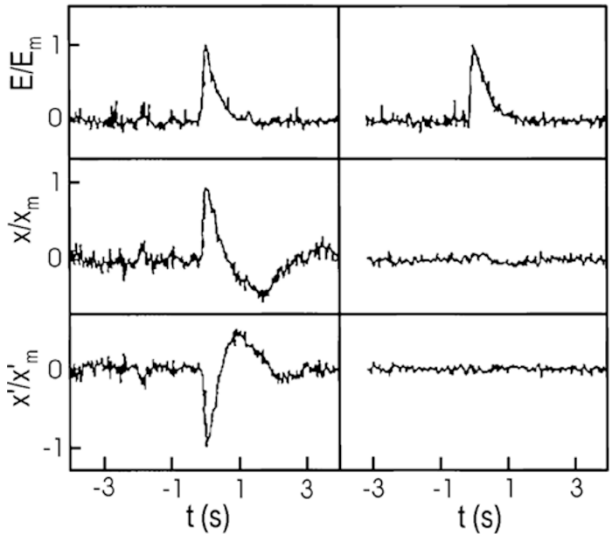

Fig. 3.21. Response of the orbit and energy feedback in the ring-to-linac transfer line of the SLC to a fast step change in energy [43]: (*left*) before and (*right*) after additional BPMs were included in the feedback loop

There are different techniques to calibrate the local transport matrices between correctors and BPMs within each feedback loop, which are used to continually compute the excitation of the feedback steering correctors. For example, the induced change in orbit position and angle can be measured as a function of the individual feedback corrector strengths.

If there are successive feedback loops on a beam line, these loops could interfere with each other, and cause unwanted orbit oscillations due to "double-compensation". This interference can be avoided by one of 4 different approaches [42]: (1) orthogonality of correction, (2) different feedback response time, (3) inter-loop communication (feedback "cascades") and (4) integration of loops into one global loop. The orbit feedbacks in the SLAC linac are connected by a so-called adaptive cascade, where each feedback passes its information to the loop downstream, in order to avoid multiple corrections of the same perturbation. The linear transport matrix between successive loops is monitored and updated continuously using the naturally occurring beam-orbit variation.

3.10 Excursion – AC Dipole

Not always is there a well defined closed orbit in a storage ring which is stable from turn to turn. As an example of a case without regular closed orbit, we consider a dipole field that is modulated at a frequency near the fractional

part of the betatron tune. We assume that the field changes on successive turns, but has a sinusoidal variation, so that it repeats after a larger number of turns. In this case there is a new dynamic 'closed orbit' which returns to its starting point after a full modulation period. The amplitude of this periodic orbit is [44]

$$\hat{x} = \frac{\beta_x (B_{\mathrm{mod}} l_{\mathrm{dip}})}{4\pi (B\rho) \Delta Q}\,, \tag{3.47}$$

where B_{mod} is the amplitude of the dipole-field modulation, l_{dip} the length of the dipole, $(B\rho)$ the magnetic rigidity, $\Delta Q = |Q_x - Q_m - k|$, Q_x the betatron tune, Q_m the modulation tune, and k an integer which minimizes ΔQ. The amplitude of the dynamic orbit increases inversely with the frequency difference of modulation and betatron oscillations. Such a dynamic closed orbit may be used to increase the strength of spin resonances in order to preserve the polarization during acceleration [45] (see also the discussion of polarization in Chap. 9) or it can aid in measuring lattice nonlinearities [44] without diluting the transverse emittance. First tests were successfully performed at the BNL AGS [44, 45] and the CERN SPS [46].

Exercises

3.1 Design of an Orbit Feedback Loop

Write an algorithm for orbit correction in one plane assuming uncoupled, linear transport. Let the beam position and angle be detected using two BPMs and use two fast corrector dipoles for implementing the desired deflections. Introduce (assumed known) relative phase advances and beta functions as needed to take into account phase differences between the correctors, between the BPMs, and between the correctors and BPMs. Comment on the optimum phase advances between the correctors and BPMs and comment on the optimum beta functions at the locations of the measurements and corrections. Consider

a) a transport line,

b) a circular accelerator.

3.2 Linac Dispersion and Orbit Correction

a) Dispersion for a free betatron oscillation. Consider a beam deflected by an angle θ at $s = 0$. In a smooth approximation, and ignoring wake field effects, the betatron motion of a single particle with relative momentum deviation δ_1 is

$$x_1''(s) + \frac{k_\beta^2}{1+\delta_1} x_1(s) = \frac{\theta}{1+\delta_1} \delta(s)\,, \tag{3.48}$$

where the last $\delta(s)$ is the Dirac delta function, indicating a single deflection of strength θ at location $s = 0$, and $k_\beta = \sqrt{K}$ is the wave number of the

betatron oscillation. Equation (3.48) describes the motion of an individual off-momentum particle in the bunch, as well as of the bunch centroid if the latter experiences a momentum offset δ_1. The equality of the particle and centroid motion (for small bunch charges) is an advantage, since the single-particle dispersion can be measured by observing the response of the centroid motion to an energy error. Solve (3.48), linearize the solution in δ_1 and determine the dispersion for $k_\beta s\delta_1 \ll 1$.

b) Dispersion behind a π bump. A one-to-one orbit correction can be thought of as a superposition of π bumps. Calculate the dispersion generated by a single π bump represented by two kicks θ, at $s_1 = 0$ and $s_2 = \pi/k_\beta$.